GEOPHYSICS, VOL. 65, NO. 2 (MARCH-APRIL 2000); P. 502–511, 10 FIGS., 1 TABLE.

Airborne resistivity and susceptibility mapping in magnetically polarizable areas

Haoping Huang* and Douglas C. Fraser‡

ABSTRACT

The apparent resistivity technique using half-space models has been employed in helicopter-borne resistivity mapping for twenty years. These resistivity algorithms yield the apparent resistivity from the measured in-phase and quadrature response arising from the flow of electrical conduction currents for a given frequency. However, these algorithms, which assume free-space magnetic permeability, do not yield a reliable value for the apparent resistivity in highly magnetic areas. This is because magnetic polarization also occurs, which modifies the electromagnetic (EM) response, causing the computed resistivity to be erroneously high. Conversely, the susceptibility of a magnetic half-space can be computed from the measured EM response, assuming an absence of conduction currents. However, the presence of conduction currents will cause the computed susceptibility to be erroneously low.

New methods for computing the apparent resistivity and apparent magnetic permeability have been developed for the magnetic conductive half-space. The in-phase and quadrature responses at the lowest frequency are first used to estimate the apparent magnetic permeability. The lowest frequency should be used to calculate the permeability because this minimizes the contribution to the measured signal from conduction currents. Knowing the apparent magnetic permeability then allows the apparent resistivity to be computed for all frequencies.

The resistivity can be computed using different methods. Because the EM response of magnetic permeability is much greater for the in-phase component than for the quadrature component, it may be better in highly magnetic environments to derive the resistivity using the quadrature component at two frequencies (the quad-quad algorithm) rather than using the in-phase and quadrature response at a single frequency (the in-phase–quad algorithm). However, the in-phase–quad algorithm has the advantage of dynamic range, and it gives credible resistivity results when the apparent permeability has been obtained correctly.

INTRODUCTION

Resistivity mapping using helicopter towed-bird frequency-domain electromagnetic (EM) systems has been used for a variety of applications. These include metallic mineral prospecting, kimberlite identification, geothermal exploration, water detection, mapping saltwater intrusion into fresh water, assessing landslide risk and other hazards, and numerous other applications where knowledge of the electrical properties of the earth is important. The apparent resistivity is typically obtained by the transformation of the measured in-phase and quadrature response and the aircraft altimeter, using techniques developed by Fraser (1978, 1990). Figure 1 shows two half-space models. Figure 1a is termed the homogeneous half-space model, and Figure 1b is the pseudolayer half-space model.

The upper (pseudo) layer of the pseudolayer half-space model of Figure 1b is merely an artifice to account for the difference between the computed sensor source height h and the measured sensor altitude a. The measured sensor altitude is determined from the radar or laser altimeter. Any error in the altimeter reading, e.g., as caused by a forest canopy, falls into the computed sensor source height and therefore does not corrupt the computed resistivity. The pseudolayer half-space is the model of choice for displaying the apparent resistivity in both plan (Fraser, 1990) and section (Sengpiel, 1988), in part because of this immunity to altimeter errors.

The differential method for helicopter-borne resistivity mapping was developed by Huang and Fraser (1996) to yield a smoothed approximation of the true-resistivity distribution with depth. The differential resistivity is derived from the

Manuscript received by the Editor March 11, 1999; revised manuscript received July 22, 1999.
*Formerly Geoterrex-Dighem, Unit 2, 2270 Argentia Rd., Mississauga, Ontario L5N 6A6, Canada; presently Geophex, Ltd., 605. Mercury St., Raleigh, North Carolina 27603. E-mail: haoping_huang@hotmail.com or huang@geophex.com.
‡Geoterrex-Dighem, Unit 2, 2270 Argentia Rd., Mississauga, Ontario L5N 6A6, Canada. E-mail: 105421.2020@compuserve.com.

apparent resistivity of the pseudolayer half-space model and is more sensitive to layering than the half-space resistivity itself. The methods used to calculate the half-space resistivity and the differential resistivity work well in areas free of magnetic polarization. However, they yield erroneous resistivities in highly magnetic areas because the in-phase and quadrature response are affected by magnetic polarization.

The effect of magnetic permeability can be obtained from the transformation of low-frequency helicopter EM data when the earth is nonconductive at the transmitted frequency. The magnetic effect on the EM data can be portrayed as a susceptibility thickness or related product (Fraser, 1973) or as a susceptibility or related product (Fraser, 1981). These methods may be used for iron ore exploration, although errors are caused by conduction currents, as discussed by Flis et al. (1998). Magnetic permeability also can be obtained from inverting multifrequency helicopter EM data (Zhang and Oldenburg, 1997) and portrayed as a susceptibility that varies with depth, providing the resistivity-depth model is known. Both resistivity and susceptibility can be obtained simultaneously from inversion, assuming homogeneous layers of known thickness (Zhang and Oldenburg, 1999). Beard and Nyquist (1998) demonstrate the utility of simultaneous inversion of helicopter EM data using a magnetic conductive layered earth. They invert for resistivity and permeability with a goal of locating buried metallic waste. They also provide interesting observations on the constancy of the so-called in-phase shift caused by magnetic permeability.

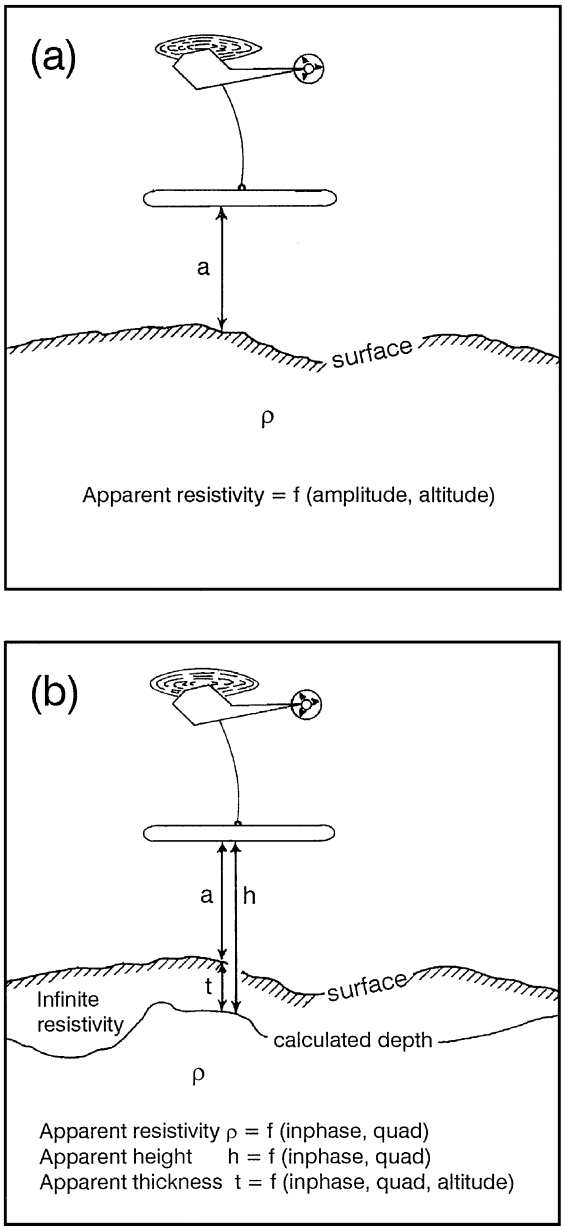

FIG. 1. (a) The homogeneous half-space model, where the top of the half-space coincides with the earth's surface as defined by the radar or laser altimeter. The amplitude refers to the square root of the sum of the squares of the in-phase and quadrature. (b) The pseudolayer half-space model, where the top of the half-space is defined numerically by the output parameter *h*. The pseudolayer half-space model is equivalent to a two-layer case where the upper layer is of infinite resistivity. The thickness *t* is the difference between the interpreted height *h* and the bird altitude *a* as obtained from the altimeter.

Magnetic permeability has much less impact on the quadrature component than on the in-phase component. This raises the concept of using the quadrature response from two adjacent frequencies (the quad-quad algorithm) to compute the resistivity by transformation to a half-space model, rather than using the in-phase and quadrature response at a single frequency (the in-phase-quad algorithm). Huang and Fraser (1998) first transform the in-phase and quadrature response at the lowest frequency to yield the approximate apparent magnetic permeability. Following this, the quad-quad algorithm is used to compute one apparent resistivity from two adjacent frequencies using the computed apparent magnetic permeability as input.

In this paper, the data transform method of Huang and Fraser (1998), using a magnetic conductive half-space model, is refined to yield the exact apparent magnetic permeability, which is then employed to obtain the apparent resistivity using the in-phase–quad algorithm. We provide field examples to show the impact of permeability on the resistivity obtained from both the in-phase–quad and quad-quad algorithms. While we use data and present figures specific to the Dighem helicopter EM system, the technique is applicable to any closely coupled airborne EM system.

BASIC EQUATIONS

The EM response of a half-space for dipole source excitation is given by Frischknecht (1967), Ward (1971), and Ward and Hohmann (1988), among others. If the transmitting and receiving coils are at a height h above a homogeneous half-space, the secondary magnetic field H_S, normalized against the primary field H_0 at the receiving coil, is

$$H_s/H_0 = s^3 \int_0^\infty \psi(\lambda)\lambda^2 \exp(-2\lambda h) J_0(\lambda s)\, d\lambda, \qquad (1)$$

where s is the coil separation and J_0 is the Bessel function of the first kind of order zero. The term $\psi(\lambda)$ can be written as

$$\psi(\lambda) = (1 - \lambda c_1)/(1 + \lambda c_1), \qquad (2)$$

where c_1 for a homogeneous half-space is

$$c_1 = \mu_r(\lambda^2 + i\varpi\sigma\mu)^{-1/2}. \qquad (3)$$

Here, λ is an integral variable, $i = \sqrt{-1}$; ω is the angular frequency $2\pi f$, where f is the frequency in Hz; σ is the

conductivity; and μ_r is the relative magnetic permeability μ/μ_0, where μ is the magnetic permeability of the earth and μ_0 is the magnetic permeability of free space. These equations make the common quasistatic assumption that conduction currents are much larger than displacement currents, i.e., $\sigma \gg \omega\varepsilon$, where ε is the dielectric permittivity. The equations also assume that μ is nondispersive and therefore frequency independent (Fraser, 1981).

For closely coupled transmitting and receiving coils, equation (1) can be approximated as (cf. Fraser, 1972)

$$H_S/H_0 = (s/h)^3[M(\theta, \mu_r) + iN(\theta, \mu_r)], \qquad (4)$$

where the secondary field response H_S is expressed in units of parts per million (ppm) of the primary field intensity H_0 at the receiving coil. The measured in-phase I and quadrature Q components in parts per million may be represented as

$$I = (s/h)^3 M \qquad \text{and} \qquad Q = (s/h)^3 N, \qquad (5)$$

where M and N, respectively, are the in-phase and quadrature components of the response function $M + iN$ and reflect the in-phase and quadrature response scaled for variations in flying height h and coil separation s. Equations (4) and (5) are valid on the assumption that $s^3 \ll h^3$. This superimposed dipole assumption (Grant and West, 1965) is generally valid for surveys flown with commercial helicopter EM systems.

Values M and N themselves are functions of the dimensionless induction number $\theta = (\omega\sigma\mu h^2)^{1/2}$ and the relative magnetic permeability μ_r. Figure 2 (Huang and Fraser, 1998) shows M and N as functions of θ for various values of μ_r for horizontal coplanar coils over a homogeneous half-space. The effect of a magnetic permeability μ greater than μ_0 is twofold. First, the permeability increases the value of the induction number θ. Second, as $\theta \to 0$, the response function $M + iN$ becomes dominated by the magnetization effect, which is in-phase with and in the same direction as the primary field. This is the induced magnetization, which occurs for an alternating magnetic field of a coil just as it does for the static magnetic field of the earth. At low induction numbers, the in-phase component M of the response function becomes frequency independent and the quadrature component N tends to zero. At the other extreme, when the induction number is large, the induced conductive response completely overwhelms the magnetization effect. All curves in Figure 2 converge to that for $\mu_r = 1$ as $\theta \to \infty$. For midrange induction numbers, the magnetization effect and conductive effect are mixed.

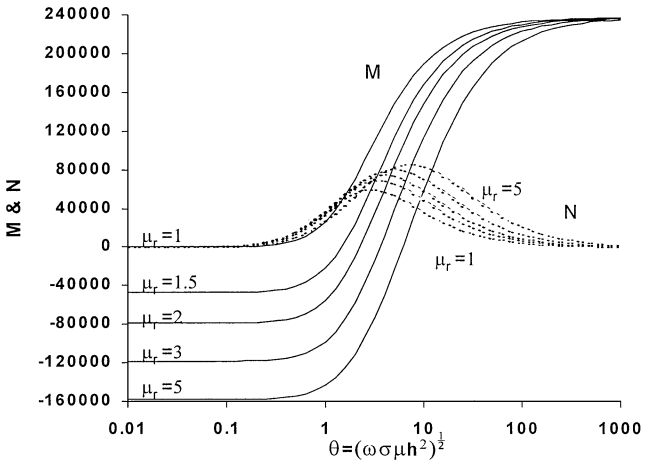

FIG. 2. In-phase M and quadrature N components of the response function of a homogeneous half-space plotted as a function of the induction number θ for various values of the relative magnetic permeability μ_r for horizontal coplanar coils.

Just as the geometric term $(s/h)^3$ cancels out in the in-phase/quadrature ratio I/Q as seen by equation (5), so it also cancels out of other response ratios. For example, the geometric term does not appear in the ratio Q_ℓ/Q_h, where Q_ℓ and Q_h represent the quadrature response at a given low and high frequency, respectively. We use this independence from the geometric term in deriving the apparent resistivity.

MAGNETIC CONDUCTIVE HALF-SPACE

The permeability and conductivity of a magnetic conductive half-space are obtained by transforming the in-phase and quadrature responses through closed solutions. We demonstrate the method graphically using Figures 3 and 4.

Determination of apparent relative permeability

The relative magnetic permeability μ_r could be obtained from the measured magnetometer data by computing the apparent susceptibility and then converting to the relative magnetic permeability μ_r. This approach is of doubtful utility because the earth's static uniform magnetic field samples the earth much differently than the alternating dipole magnetic field of the transmitting coil, and remanence may also exist for the static field. Consequently, we prefer to obtain the relative magnetic permeability from the observed EM data at the lowest available induction number, i.e., at the lowest frequency.

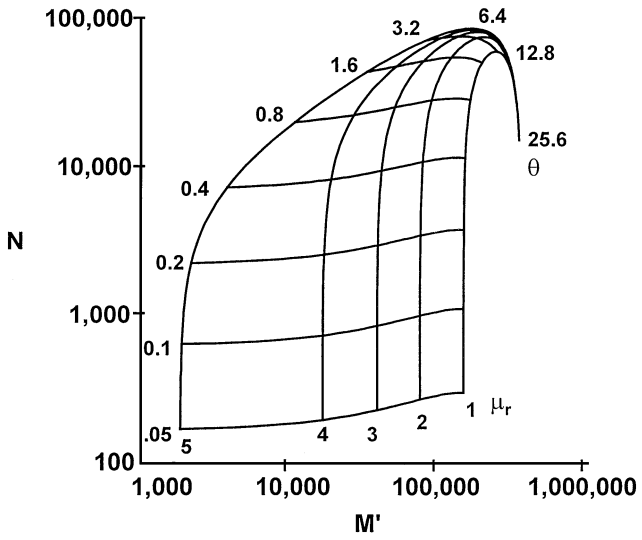

FIG. 3. The phasor diagram of the in-phase M' and quadrature N components for the half-space model of a magnetic conductive earth for several induction numbers θ and relative permeabilities μ_r. To plot the diagram in log space, M' is taken as $M + 160\,000$ to ensure that all in-phase data are positive. The base value of 160 000 is determined from Figure 2 as the smallest in-phase value for μ_r up to 5.

Fraser (1981) describes a magnetite mapping technique based on the transformation of the negative in-phase response, which is valid when the quadrature response is zero, i.e., when the earth is nonconductive at the transmitted frequency. Figure 2 shows that the in-phase M of the response function is dependent only on the relative permeability μ_r as the induction number $\theta \to 0$, which occurs when there are no conduction currents. However, in this paper we obtain the relative magnetic permeability by using both the in-phase and quadrature response with a method that is applicable in the presence of conduction currents.

To calculate the apparent permeability, the in-phase M and quadrature N components are first obtained from equation (5) on the assumption that the bird altitude a can be used in place of the unknown sensor source height h. The relative magnetic permeability is then obtained from Figure 3, which is the phasor diagram for the half-space model of a magnetic conductive earth. This diagram yields the induction number θ and relative permeability μ_r, given the quantities M' and N. M' is simply M plus a base value of 160 000, which is added to keep this quantity positive. The permeability μ_r can be well resolved when the induction number θ is low—indeed, the permeability depends only upon the in-phase response when $\theta < 0.1$. The permeability cannot be resolved from the diagram when $\theta > 4$.

The induction number θ from Figure 3 indicates the resolvability of the relative permeability μ_r. If θ is low, the value of μ_r from Figure 3 is likely to be reliable. If θ is greater than four, the relative permeability μ_r will not be reliable. This induction number θ is obtained using a homogeneous half-space model (Figure 1a) since Figure 3 assumes that the bird altitude from the altimeter can be used in place of the unknown sensor source height. This θ is not the same as the induction number θ from the pseudolayer half-space model (Figure 1b), which is used to obtain resistivity.

If the earth is a true homogeneous magnetic conductive half-space, the relative magnetic permeability μ_r obtained from Figure 3 would be the true relative permeability. Otherwise, it would be the apparent relative permeability.

In practice, the above procedure should be followed using data from the lowest frequency to ensure that the induction number θ is as low as possible to maximize the ratio of magnetic response to conductive response. A frequency of 900 Hz is common to all Dighem systems, while some of these systems use 220 or 385 Hz as the lowest frequency. With a resistivity of 2 ohm-m (which is very conductive, being one-eighth the conductivity of sea water), a relative magnetic permeability of 3 (which is very magnetic, representing approximately 40 vol % magnetite) and a frequency of 900 Hz, the induction number θ is 4.1 for a sensor altitude of 40 m (which is higher than the normal altitude of 30 to 35 m). Thus, the induction number condition of $\theta < 4$ is satisfied for most survey environments, so Figure 3 is generally applicable for Dighem surveys.

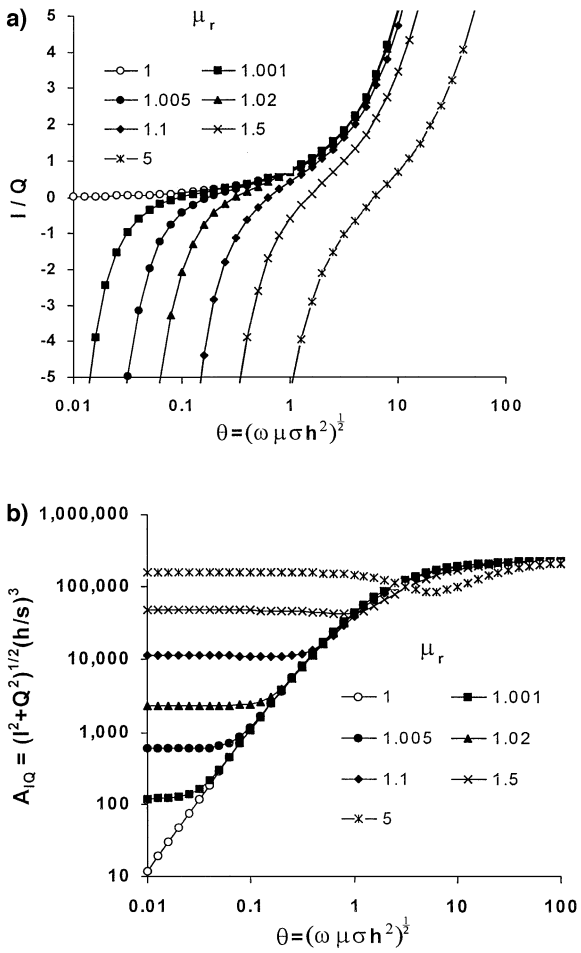

FIG. 4. (a) The ppm ratio I/Q and (b) the normalized amplitude A_{IQ} as functions of θ for various values of the relative magnetic permeability μ_r.

Determining apparent resistivity using the in-phase–quad algorithm

The apparent resistivity can be determined from the in-phase–quad algorithm for each individual frequency following the above computation of the relative magnetic permeability μ_r. Given μ_r, we use Figure 4a to obtain the induction number $\theta = (\omega\sigma\mu h^2)^{1/2}$ from the ratio of the in-phase I and quadrature Q for a given frequency $\omega = 2\pi f$. Knowing θ, we then obtain the normalized amplitude $A_{IQ} = (M^2 + N^2)^{1/2} = (I^2 + Q^2)^{1/2}\ (h/s)^3$ from Figure 4b. This allows the apparent height h (see Figure 1b) to be calculated from

$$h_a = s\left[A_{IO}/(I^2 + Q^2)^{1/2}\right]^{1/3}. \tag{6}$$

The apparent thickness (Figure 1b) and apparent resistivity for each individual frequency f are obtained from

$$t_a = h_a - a \tag{7}$$

and

$$\rho = 2\pi\mu f(h_a/\theta)^2, \tag{8}$$

where a is the EM bird altitude obtained from the altimeter and the resistivity ρ is the reciprocal of the conductivity σ. In equation (8), $\mu = \mu_r\mu_0$, where μ_r is obtained from Figure 3.

Equations (6)–(8), along with Figure 4, transform the observed in-phase and quadrature responses of a single frequency to the apparent thickness and apparent resistivity of the

pseudolayer half-space model. If the earth is truly homogeneous, the resistivity obtained from equation (8) is the true resistivity ρ. Otherwise, it is the apparent resistivity ρ_a.

Determining apparent resistivity using the quad-quad algorithm

We show synthetic and field data below where the computed resistivity is compared using both the in-phase–quad and the quad-quad algorithms. The quad-quad transformation method is quite similar to the in-phase–quad method. We use the quadrature ratio Q_ℓ/Q_h from two adjacent frequencies f_ℓ and f_h rather than the in-phase–quad ratio at a single frequency. The normalized amplitude $A_{QQ} = (N_\ell+N_h) = (Q_\ell+Q_h)(h/s)^3$ uses these two quadrature responses. A quad-quad figure analogous to Figure 4 is given in Huang and Fraser (1998). The apparent height h_a is obtained as $h_a = s[A_{QQ}/(Q_\ell + Q_h)]^{1/3}$, and the apparent thickness and apparent resistivity for the pair of frequencies are obtained from the equations (7) and (8), where f and θ in equation (8) are replaced by the low-frequency f_ℓ and θ_ℓ.

TESTS ON SYNTHETIC DATA

We have compared the in-phase–quad and quad-quad algorithms for a variety of magnetic conductive layered earths. We refer to the apparent resistivities obtained from the quad-quad technique as the quad-quad resistivity and the apparent resistivities from the single-frequency in-phase–quad technique as the in-phase–quad resistivity. The methods return the correct values of permeability and resistivity for homogeneous half-spaces. For a two-layered earth, however, some undesirable effects can result. We present three representative two-layer cases.

We first examine two two-layer cases, one having an upper conductive layer (Figure 5) and the other having an upper resistive layer (Figure 6). The thickness of the upper layer for each model increases from left to right. For each model, we show the in-phase–quad and quad-quad resistivities for a number of discrete permeabilities. In the interest of reducing the number of variables, the upper-layer permeability has been kept the same as the lower-layer permeability.

In Figures 5 and 6, panels (a) and (b) display the in-phase–quad resistivities for 56 000 Hz and 900 Hz, respectively. The apparent resistivity for the intermediate Dighem frequency of 7200 Hz is not shown. Panels (c) and (d), respectively, display the quad-quad resistivities for the 7200–56 000-Hz pair of frequencies and for the 900–7200-Hz pair.

In generating Figures 5 and 6, the forward solutions yielded the in-phase and quadrature responses for the various frequencies. The permeability was first determined from the 900-Hz EM data. The permeability was then used along with the EM responses to obtain the apparent resistivity using the in-phase–quad and quad-quad algorithms. Typical examples of the output permeability are shown in Table 1. This table shows that the permeability is obtained relatively correctly even though the resistivity varies in this two-layer case having constant permeability. The resistivity of the upper layer is 50 ohm-m, and that of the lower layer is 500 ohm. The relative magnetic permeability μ_r of both layers is the same, being either 1.5, 2, or 3. The computed apparent relative permeabilities μ_{ra} are close to the true values.

The resistivity curves of Figures 5 and 6 illustrate that the apparent resistivities are affected by the permeability. Thus, when $\mu_r > 1$, the transformation yields permeability-dependent values for the apparent resistivities, even when the correct permeability is used in the transformation to the half-space model. We can use the expression nonpermeable apparent resistivity to refer to the apparent resistivity which is obtained for the nonmagnetic curve of $\mu_r = 1$. When $\mu_r > 1$, an apparent resistivity identical to the nonpermeable resistivity cannot be obtained through the transformation process when using half-space models although it can be close to it, as seen in these figures.

The apparent resistivity curves for $\mu_r > 1$ are mainly located below the nonpermeable apparent resistivity curves in Figure 5. This means that the magnetic permeability makes the earth appear to be more conductive than the nonpermeable apparent resistivity for this two-layer case. Permeability apparently causes the EM data to bias the computed results toward the upper-layer resistivity. This results partly from the skin depth phenomenon, since permeability reduces skin depth in proportion to its inverse square root, thereby biasing the current flow to the upper layer. This biasing behavior is more acute for the in-phase–quad algorithm (Figures 5a, b) than for the quad-quad algorithm (Figures 5c, d). The biasing of the quad-quad resistivity is generally not serious when the relative magnetic permeability is <2, i.e., when the amount of magnetite is less than about 20% by volume. Magnetic rocks seldom contain this much magnetite. Thus, there is a strong reason for using the quad-quad algorithm in magnetic terrain, notwithstanding the danger of resistivity undershoot or overshoot which can occur.

The quad-quad resistivity for 7200 Hz/56 000 Hz lies outside the range of the true resistivities of the two-layer model of Figure 5, at $t_1 \approx 12$ m, for large values of the relative permeability. The reason for the undershoot of the 7200 Hz/56 000 Hz quad-quad resistivity is related to skin depth. For a two-layer case, a resistivity overshoot or undershoot tends to occur when the two-layer interface is about 1.5 times deeper than the skin depth of the upper-layer resistivity for the higher frequency. For single-frequency analysis using the in-phase–quad algorithm, the apparent resistivity may also overshoot or undershoot for an interface at the same depth (e.g., Figure 6a). We have found that a resistivity undershoot or overshoot tends to be more prevalent with the quad-quad algorithm, and that it increases with permeability (Figures 5c and 6a).

Our third example of synthetic data uses a model similar to Figure 5 except that the upper layer of Figure 7 is nonmagnetic

Table 1. Transformation results using a pseudolayer half-space model on data from a two-layer earth for various thicknesses t_1 of the upper layer in *m*.

t_1	μ_r	μ_{ra}	μ_r	μ_{ra}	μ_r	μ_{ra}
1	1.5	1.5012	2	2.0027	3	3.0073
2	1.5	1.5029	2	2.0060	3	3.0160
3	1.5	1.5047	2	2.0093	3	3.0236
5	1.5	1.5080	2	2.0154	3	3.0388
10	1.5	1.5146	2	2.0280	3	3.0705
30	1.5	1.5238	2	2.0438	3	3.1025
50	1.5	1.5193	2	2.0328	3	3.0659
100	1.5	1.5048	2	2.0055	3	3.0040
∞	1.5	1.5000	2	2.0000	3	3.0000

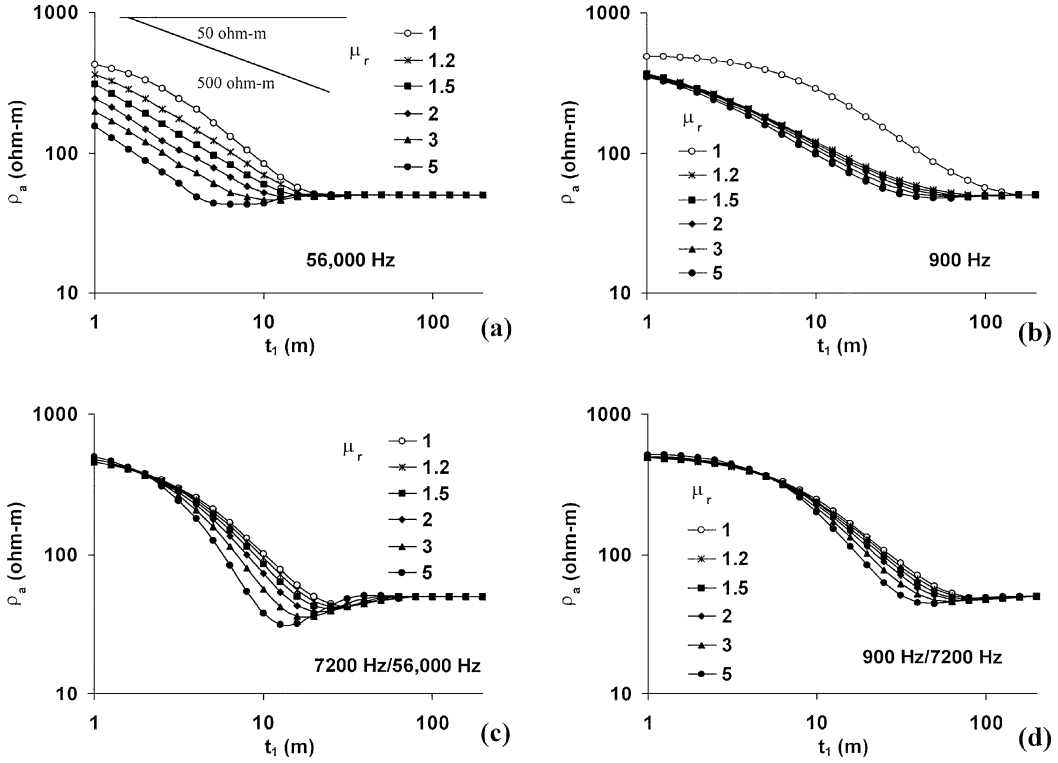

FIG. 5. The apparent resistivity is shown for several permeabilities using the in-phase–quad algorithm for (a) 56 000 and (b) 900 Hz, and for the quad-quad algorithm for (c) 7200 and 56 000 Hz and for (d) 900 and 7200 Hz. The two-layer model has an upper-layer resistivity of 50 ohm-m and a lower-layer resistivity of 500 ohm-m. The upper layer increases thickness to the right along the *x*-axis. The permeability is the same for each layer.

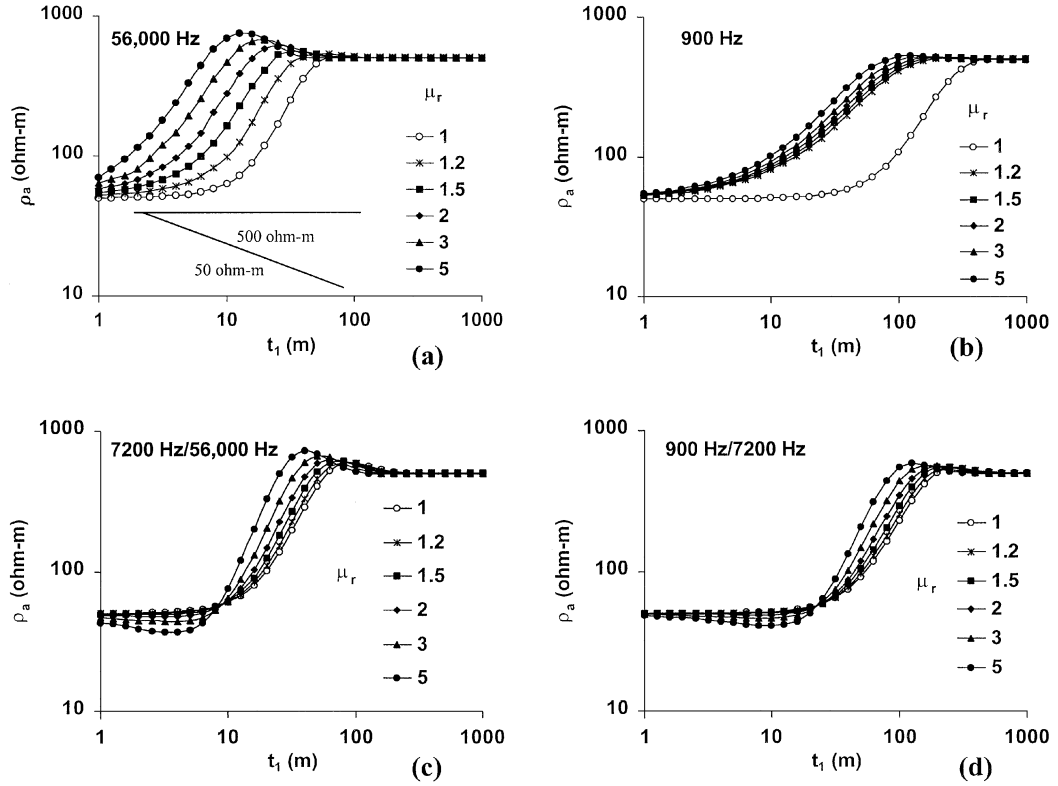

FIG. 6. The apparent resistivity is shown for several permeabilities using the in-phase–quad algorithm for (a) 56 000 and (b) 900 Hz, and for the quad-quad algorithm for (c) 7200 and 56 000 Hz and for (d) 900 and 7200 Hz. The two-layer model has an upper-layer resistivity of 500 ohm-m and a lower-layer resistivity of 50 ohm-m. The upper layer increases thickness to the right along the *x*-axis. The permeability is the same for each layer.

and the relative magnetic permeability μ_r of the lower layer varies discretely from 1 to 5. The model is shown in Figure 7a; Figure 7b shows the apparent susceptibility $\kappa_a = \mu_{ra} - 1$ computed from the 900-Hz EM data for each of the five discrete permeabilities of the lower layer. The apparent magnetic susceptibility is shown, rather than the apparent relative permeability, to provide a greater sensitivity to the display. When the cover is thin (e.g., 1 m), the computed susceptibility is very close to the true susceptibility of the lower layer. However, for a 100-m-thick cover of conductive, nonmagnetic material, the computed susceptibility is vanishingly small. The computed values of the relative magnetic permeability were used, along with the in-phase and quadrature responses for the various frequencies, to compute the in-phase–quad resistivities shown in Figures 7c, d and the quad-quad resistivities shown in Figures 7e, f. Note the qualitative similarity in the various apparent resistivities of Figures 5 and 7. For example, the 56 000-Hz in-phase–quad resistivity of Figure 5a behaves similarly to that of Figure 7c, and the 900-Hz/7200-Hz quad-quad resistivity of Figure 5d is similar to that of Figure 7f.

TESTS ON REAL DATA

A proper assessment of the pros and cons of the in-phase–quad and quad-quad resistivity algorithms would involve the presentation of many model cases, which is beyond the scope

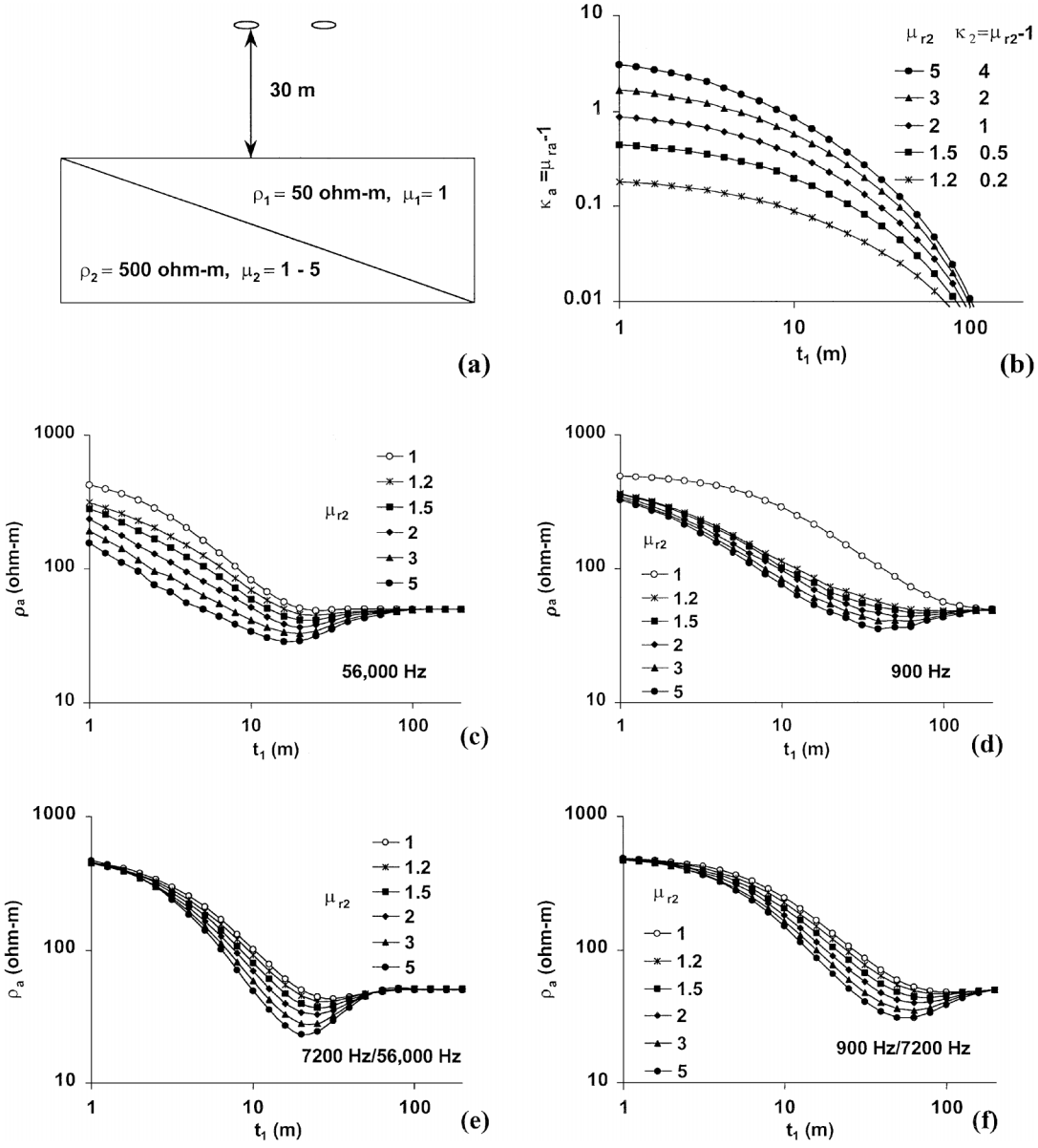

FIG. 7. (a) The two-layer model has a nonmagnetic upper layer resistivity of 50 ohm-m, a discretely variable magnetic lower-layer resistivity of 500 ohm-m, and a continuously variable thickness of the upper layer as shown on the x-axis. (b) The apparent magnetic susceptibilities κ are calculated from the 900-Hz data. The apparent resistivities are shown for the various lower-layer permeabilities using the in-phase–quad algorithm for (c) 56 000 and (d) 900 Hz and using the quad-quad algorithm for (e) 7200 and 56 000 Hz and (f) 900 and 7200 Hz.

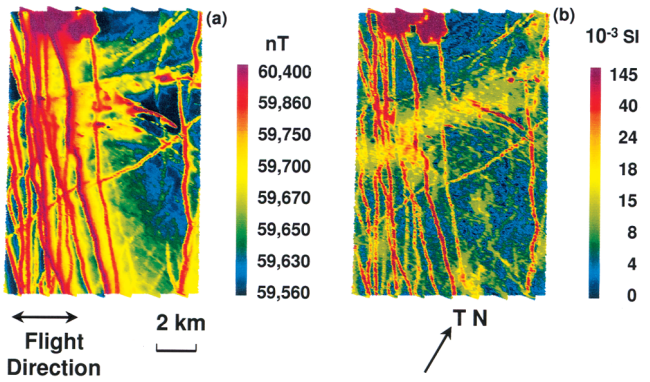

FIG. 8. The results from a helicopter survey area in Canada's far north, showing (a) the static total magnetic field as measured by a magnetometer and (b) the magnetic susceptibility calculated from the 900-Hz Dighem EM data.

of this paper. Alternatively, we can view examples of field data. Field examples tend to encompass many resistivity and permeability variations in a single survey. While they may not provide a good understanding of the physical reality, they can at times provide a qualitative view of the usefulness of an analytic method.

Our first field example is from an area where the geology is steeply dipping and the overburden is quite thin. In this example, we only show the magnetic susceptibility map (from the EM) and the associated total field magnetic map (from the magnetometer) because the purpose of this example is to indicate the usefulness of the EM-derived susceptibility mapping technique. Figure 8 shows (1) the total field magnetic map and (2) the EM-derived magnetic susceptibility map from a Dighem survey in Canada's far north. The main magnetic features, as indicated by dike and fault patterns, are similar for both maps. This similarity between the total field magnetic map

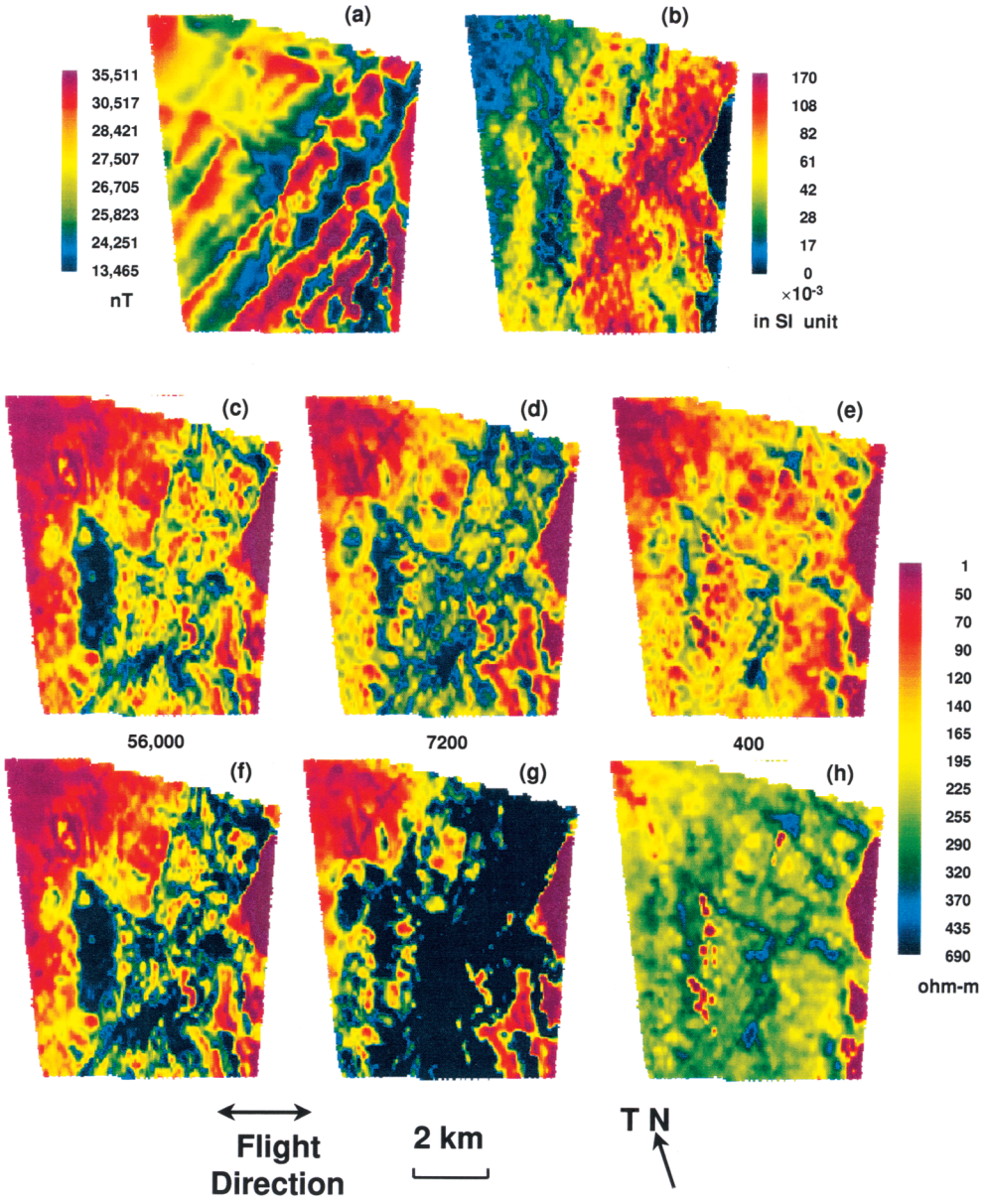

FIG. 9. The results from a helicopter survey area in Africa showing (a) the static total magnetic field as measured by a magnetometer and (b) the magnetic susceptibility calculated from the 400-Hz Dighem EM data. Shown are the in-phase–quad resistivity maps for (c) 56 000 Hz, (d) 7200 Hz, and (e) 400 Hz, where the input apparent permeability is the same as that used to produce the apparent susceptibility map of panel (b). Also shown are the in-phase–quad resistivity maps for (f) 56 000 Hz, (g) 7200 Hz, and (h) 400 Hz, where the input apparent permeability is assumed to be that of free space.

and the EM-derived magnetic susceptibility map is expected since the lithology is steeply dipping and the overburden is thin. In this case, both the helicopter EM system and the magnetometer are virtually sampling the same geology even though the depth of exploration of the magnetometer is much greater than that of the helicopter EM system.

The EM-derived magnetic susceptibility of Figure 8b displays a higher resolution of the minor features than the total field magnetic map of Figure 8a. This is evident in the eastern portion of the survey area. The higher resolution for the EM-derived susceptibility is not surprising since the dipole magnetic field of the EM transmitting coil has a higher resolution than the uniform magnetic field of the earth.

Our second field example is from an area in southern Africa where the strata are gently dipping and highly magnetized in places and where the overburden is conductive with a variable thickness. Figure 9 shows the total field magnetic map, the EM-derived apparent magnetic susceptibility, and various in-phase–quad resistivity maps from a Dighem survey in which the three frequencies of the coplanar coil pairs are 400, 7200, and 56 000 Hz. The in-phase data at 400 Hz are commonly negative in the resistive areas, responding to relatively strong magnetic polarization. Figure 9b shows the apparent susceptibility map obtained from the 400-Hz EM data. This map looks quite different from the corresponding total field magnetic map of Figure 9a, primarily because the EM and magnetometer sensors have sampled quite different geology because of their dramatically different depths of exploration. Thus, the EM data reflect only the near-surface magnetic properties, while the magnetometer sees much deeper. Other less significant differences are (1) the resolution of the EM method is higher than the magnetometer method as referred to above; (2) the EM sensor responds only to induced magnetization while the magnetometer responds to both induced and remnant magnetization; and (3) the inclination and declination of the inducing flux of the EM transmitting coil is independent of its location on the earth's surface, unlike that of the earth's magnetic field.

The in-phase–quad resistivity maps are shown in Figures 9c, d, and e for 56 000 Hz, 7200 Hz, and 400 Hz, respectively. These apparent resistivities were computed using input permeabilities corresponding to the apparent susceptibilities shown in Figure 9b. For comparison, the in-phase–quad resistivities for the three frequencies are also shown, assuming free-space permeability in Figures 9f, g, and h. A comparison of Figures 9c and 9f, of Figures 9d and 9g, and of Figures 9e and 9h illustrates that the in-phase–quad resistivity changes significantly with the input permeability. These comparisons illustrate that the output in-phase–quad resistivity is not forgiving of errors in the input permeability.

The quad-quad resistivity maps for the same area as Figure 9 are shown in Figures 10a,b for 7200 Hz/56 000 Hz and 400 Hz/7200 Hz. These apparent resistivities were computed using the permeabilities corresponding to the apparent susceptibilities shown in Figure 9b. For comparison, the quad-quad resistivities are also shown, assuming free-space permeability in Figures 10c, d. A comparison of Figures 10a and 10c and of Figures 10b and 10d illustrates that the quad-quad resistivity changes little with permeability. These comparisons show that the output quad-quad resistivity is quite forgiving of errors in the input permeability.

CONCLUSIONS

New methods for computing the apparent resistivity and apparent magnetic permeability have been developed for closely coupled helicopter-borne EM systems. The magnetic conductive half-space model is used, along with the lowest available EM frequency, to estimate the apparent magnetic permeability. This is followed by the computation of the apparent resistivity from the in-phase and quadrature EM data at a given frequency (the in-phase–quad resistivity) using the precomputed apparent magnetic permeability. Alternatively, the quadrature EM data at two frequencies can be used to compute the apparent resistivity (the quad-quad resistivity). Both the in-phase–quad resistivity and the quad-quad resistivity are apparent resistivities obtained from the pseudolayer half-space model. The true permeability and resistivity can be recovered from the in-phase–quad or quad-quad data if the earth is a truly homogeneous magnetic conductive half-space.

If the earth is not a homogeneous half-space and is nonmagnetic, the in-phase–quad resistivity algorithm is to be preferred because it provides a greater dynamic range than the quad-quad algorithm. However, if the inhomogeneous earth is magnetic, the quad-quad resistivity algorithm often will yield superior results because it is less dependent on the input value of the magnetic permeability.

The magnetic conductive half-space methods expand the use of half-space models for resistivity mapping in magnetic terrains. However, they still involve assumptions, not the least

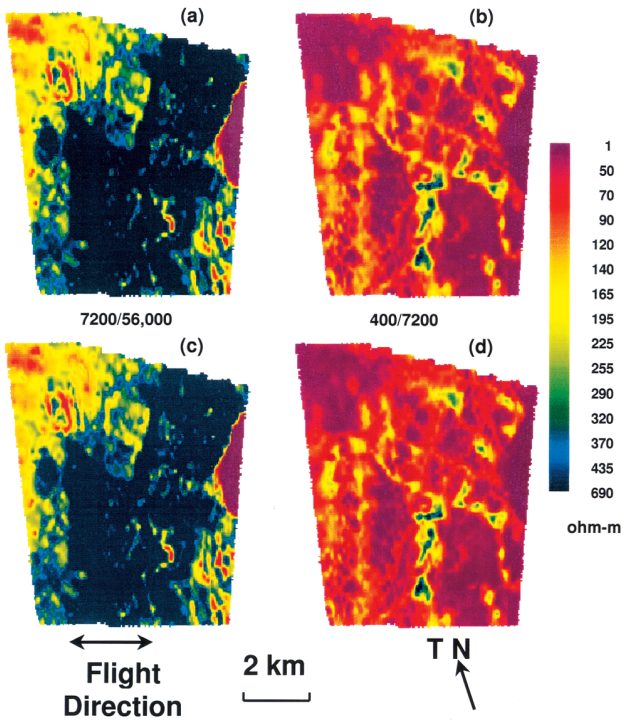

FIG. 10. The map area is the same area as for Figure 9. The quad-quad resistivity maps are shown for (a) 7200 and 56 000 Hz and for (b) 400 and 7200 Hz, where the input apparent permeability was the same as that used to produce Figure 9b. The quad-quad resistivity maps in (c) for 7200 and 56 000 Hz and in (d) for 400 and 7200 Hz reflect an input permeability of free space.

of which is the use of the half-space model itself. The use of apparent permeability in computing the apparent resistivity provides only a first-order correction since the method returns but a single value of the apparent permeability per station compared with the apparent resistivities, which vary with frequency and hence with depth. True inversion to a multilayer magnetic conductive earth is the goal of researchers in this field. For the present, however, reliable methods are not yet available for rapid data processing to yield multilayer inversions with permeability, conductivity, and thickness as variables. From a practical view, routine processing requires speed, and multilayer inversions are currently slower on fast PCs than the speed of data acquisition. Speed is important because it is desirable for in-field data processing to keep pace with data acquisition.

ACKNOWLEDGMENTS

Appreciation is expressed to Richard Smith and Peter Wolfgram for their helpful suggestions and to Geoterrex–Dighem for permission to publish this paper. We are grateful to Anglo American Corp. of South Africa Ltd. and to Tahera Corp. (formerly Lytton Minerals Ltd.) for permission to use their Dighem survey data to show the results from the analytic techniques presented in this paper.

REFERENCES

Beard, L. P., and Nyquist, J. E., 1998, Simultaneous inversion of airborne electromagnetic data for resistivity and magnetic permeability: Geophysics, **63**, 1556–1564.

Flis, M., Hawke, P., and McMillan, A., 1998, The application of multifrequency airborne electromagnetics to iron exploration: Expl. Geophys., **29**, 254–258.

Fraser, D. C., 1972, A new multicoil aerial electromagnetic prospecting system: Geophysics, **27**, 518–537.

——— 1973, Magnetite ore tonnage estimates from an aerial electromagnetic survey: Geoexploration, **11**, 97–105.

——— 1978, Resistivity mapping with an airborne multicoil electromagnetic system: Geophysics, **43**, 144–172.

——— 1981, Magnetite mapping with a multicoil airborne electromagnetic system: Geophysics, **46**, 1579–1593.

——— 1990, Layered-earth resistivity mapping, *in* Fitterman, D. V., Ed., Developments and applications of modern airborne electromagnetic surveys: U.S. Geol. Surv. Bull. **1925**, 33–41.

Frischknecht, F. C., 1967, Fields about an oscillating magnetic dipole over a two-layer earth and application to ground and airborne electromagnetic surveys: Q. Colorado School Mines, **62**, No. 1.

Grant, F. S., and West, G. F., 1965, Interpretation theory in applied geophysics: McGraw-Hill Book Co. (Div. of McGraw-Hill, Inc.).

Huang, H., and Fraser, D. C., 1996, The differential parameter method for multifrequency airborne resistivity mapping: Geophysics, **61**, 100–109.

——— 1998, Magnetic permeability and electrical resistivity mapping with a multifrequency airborne EM system: Expl. Geophys., **29**, 249–253.

Sengpiel, K. P., 1988, Approximate inversion of airborne EM data from a multilayered ground: Geophys. Prosp., **36**, 446–459.

Ward, S. H., 1971, Electromagnetic theory for geophysical applications **1**, *in* Ward, S. H., Ed., Mining geophysics: Soc. Expl. Geophys., 13–196.

Ward, S. H., and Hohmann, G. W., 1988, Electromagnetic theory for geophysical application, *in* Nabighian, M. N., Ed., Electromagnetic methods in applied geophysics, **1**: Soc. Expl. Geophys., 130–311.

Zhang, Z., and Oldenburg, D. W., 1997, Recovering magnetic susceptibility from electromagnetic data over a one-dimensional earth: Geophys. J. Internat., **130**, 422–434.

——— 1999, Simultaneous reconstruction of 1-D susceptibility and conductivity from electromagnetic data: Geophysics, **64**, 33–47.